

Subaru Spectroscopy of the Giant Ly α Nebula Associated with the High- z Powerful Radio Galaxy 1243+036¹

Youichi Ohyama², Yoshiaki Taniguchi³

²*Subaru Telescope, National Astronomical Observatory of Japan, 650 N. A'ohoku Place, University Park, Hilo, HI 96720*

³*Astronomical Institute, Graduate School of Science, Tohoku University, Aramaki, Aoba, Sendai 980-8578, Japan*

ABSTRACT

We report results of our new spatially-resolved, optical spectroscopy of the giant Ly α nebula around a powerful radio galaxy 1243+036 (4C+03.24) at $z = 3.57$. The nebula is extended over ~ 30 kpc from the nucleus, and forms a pair of cones or elongated bubbles. The high-velocity (~ -1000 km s⁻¹; blueshifted with respect to the systemic velocity) Ly α -emitting components are detected at both sides of the nucleus along its major axis. The northwestern nebula is more spectacular in its velocity shift (blueshifted by -1000 km s⁻¹ to -1400 km s⁻¹) and in its width ($\simeq 1900$ km s⁻¹ FWHM) over $\simeq 30$ kpc scale. We discuss possible origin of the nebula; 1) the shock-heated expanding bubble or outflowing cone associated with the superwind activity of the host galaxy, 2) halo gas photoionized by the anisotropic radiation from the active galactic nuclei (AGN), and 3) the jet-induced star-formation or shock. The last possibility may not be likely because Ly α emission is distributed out of the narrow channel of the radio jet. We show that the superwind model is most plausible since it can explain both the characteristics of the morphology (size and shape) and the kinematical structures (velocity shift and line width) of the nebula although the photoionization by AGN may contribute to the excitation to some extent.

Subject headings: galaxies: individual (1243+036 = 4C+03.24) – galaxies: evolution – galaxies: formation – galaxies: starburst

¹Based on data collected at Subaru Telescope, which is operated by the National Astronomical Observatory of Japan.

1. INTRODUCTION

It is well known that images of the rest-frame UV and optical continua are elongated preferentially along the radio axis in powerful radio galaxies (PRGs) at redshift (z) > 0.6 (e.g., Chambers et al. 1987; McCarthy et al. 1987); the so-called alignment effect. Indeed, many high- z ($z > 2$) PRGs (HzPRGs) show the alignment effect, and its origin has been in debate in this decade (e.g., McCarthy 1993). Various models have been proposed to explain the alignment effect; e.g., (1) scattering of the anisotropic radiation from a central engine of active galactic nuclei (AGN: e.g., di Serego Alighieri et al. 1989; Fabian 1989; Cimatti et al. 1998), (2) the jet-induced star formation (e.g., Chambers et al. 1987; McCarthy et al. 1987), and (3) the jet-induced shock heating (e.g., De Breuck et al. 2000). In these models, AGNs play some important roles to create an extended aligned continuum emission at various wavelengths. The nebula contribution to the extended UV continua is also suggested in some PRGs (e.g., Dickson et al. 1995).

An alternative idea, a pair of elongated bubbles or bi-directional cones associated with the superwind/starburst activity of the host galaxy, is proposed to explain a figure-8 shaped extended nebula in another radio galaxy, MRC 0406-244, at $z = 2.4$ (Taniguchi et al. 2001; see also Rush et al. 1997; Pentericci et al. 2001). Although the radio-jet activity and the starburst/superwind activity are different physical processes and their timescales are also significantly different, the alignment effect can be understood in the following way (Taniguchi et al. 2001). The superwind could blow as a bipolar wind, which is often observed in many superwind galaxies in the local universe (see Heckman et al. 1990), since it is likely that the gas in the host galaxy is distributed with a disk-like configuration even for a young host galaxy of HzPRGs. The radio jet is also expelled to the two directions perpendicular to the accretion plasma disk. Therefore, we can explain the alignment effect if the accretion disk is nearly co-planer to the host gas disk. Since some of these objects are known to experience vigorous star formation activity (e.g., Dey et al. 1997), this new mechanism can be regarded as one of possible ideas.

Study of such superwind nebulae in high- z universe seems very useful to understand the formation and evolution of galaxies from a general point of view. The reason for this is that galaxies are expected to experience the galactic wind (i.e., the powerful initial superwind in a late phase of the galaxy formation), which is considered to play significant roles to determine global characteristics of the present-day massive elliptical galaxies (e.g., Arimoto & Yoshii 1987). Since we know many HzPRGs even at redshift $z \gtrsim 3$ (e.g., Röttgering 1997; van Ojik et al. 1997; van Breugel et al. 1999, De Breuck et al. 2002) thanks to their powerful radio emission, their superwind activities can be used to probe early star formation history in their host galaxies. Powerful 8-10 m-class telescopes enable us to investigate them in detail (e.g.,

Villar-Martin et al. 2000).

In this paper, we focus our attention to one of HzPRGs, 1243+036 (= 4C+03.24), at $z = 3.6$, which has the aligned $\text{Ly}\alpha$ nebula, and is one of the highest- z objects known to show an alignment effect (see, e.g., Chambers et al. 1990; Lacy et al. 1994). This object was identified as a HzPRG during the course of spectroscopic survey of ultra steep spectrum sources conducted at ESO (Röttgering 1994, 1995, 1997; van Ojik et al. 1997). Its detailed follow-up observations were made by van Ojik et al. (1996; hereafter vO96). According to vO96, the observational properties of the nebula are very complex in morphology and kinematics, and can be summarized as follows². (a) This object is surrounded by a huge $\text{Ly}\alpha$ halo which extends over 135 kpc. (b) Its $\text{Ly}\alpha$ luminosity amounts to $L(\text{Ly}\alpha) \simeq 10^{44.5} h_{0.5}^{-2} \text{ ergs s}^{-1}$. (c) Its morphology shows the alignment effect. (d) Its kinematical properties show the presence of the following two components; i) the high-velocity width component with FWHM (full width at half maximum) $\simeq 1500 \text{ km s}^{-1}$ at -1100 km s^{-1} (blueshifted), and ii) the halo component with FWHM $\simeq 250 \text{ km s}^{-1}$. The halo component extends over 135 kpc with an average velocity gradient of $\simeq 450 \text{ km s}^{-1}/135 \text{ kpc}$. In addition, recent high-resolution images of R -band, K_s -band, and narrow-band near $2.3\mu\text{m}$ (corresponding to the rest-frame UV-optical continua and redshifted [OIII]4959, 5007Å emission line, respectively) have revealed closely-aligned continuum and line emission along the narrow channel of the radio jet (van Breugel et al. 1998; Pentericci et al. 1999). Although the close spatial coincidence between the UV/optical and radio emission strongly suggests a possibility of the radio jet-induced alignment component in this object, the fan- or cone-like appearance of the $\text{Ly}\alpha$ nebula seems to indicate the presence of another nebula component within the same object. Therefore it is interesting to investigate this object in more detail and to explore its origin unambiguously.

2. OBSERVATION AND DATA REDUCTION

Observation was made with the Faint Object Camera And Spectrograph, FOCAS (Kashikawa et al. 2002), attached at the Cassegrain focus of the Subaru telescope (Kaifu 1998) on April 22, 2002 (UT) to study the $\text{Ly}\alpha$ nebula around 1243+036. The sky condition was clear and the seeing size (FWHM) was 0."6. A 300 second V -band image, which includes the redshifted $\text{Ly}\alpha$ emission at $\simeq 5560\text{Å}$, was obtained without CCD binning (0."1 per pixel)

²In this paper, we assume a Hubble constant of $H_0 = 50 \text{ km s}^{-1} \text{ Mpc}^{-1}$ and a deceleration parameter of $q_0 = 0.5$ for consistency with the previous study of vO96. With these cosmological parameters, 1 arcsecond corresponds to 6.8 kpc at a distance of 1243+036.

just before the spectroscopic observation for target acquisition purpose. Then, a $0.''8$ long slit was placed on the peak of the V -band image at a position angle (PA) of 152° . The slit positioning accuracy was estimated to be about $0.''5$ due to the faintness of the target. 3×2 pixel² CCD binning was applied at the time of spectroscopy, and a single 1800 sec exposure was taken to give a spectrum covering from 4700\AA to 9400\AA with the combination of both the medium-dispersion grism (300B) with $300 \text{ grooves mm}^{-1}$ and the order sorting filter (Y47). The resultant resolution was $0.''3$ in space and 2.81\AA in wavelength per pixel corresponding 150 km s^{-1} at the redshifted $\text{Ly}\alpha$ emission. The data reduction was made by using both the IDL-based FOCAS data reduction software (Yoshida et al. 2000) and the IRAF in a standard way (overscan subtraction, bias subtraction, and flat fielding by using the dome flat images). The wavelength calibration was made by using sky emission lines, and could be done with high accuracy ($\simeq 6\text{\AA}$) because the redshifted $\text{Ly}\alpha$ emission is very close to the strong [O I] sky emission at 5577\AA .

3. RESULTS

3.1. Overall Morphology of the $\text{Ly}\alpha$ Nebula

We show our V -band image overlaid on the continuum image taken with a F702W filter of HST (Pentericci et al. 1999) in Figure 1. The V -band image is smoothed by Gaussian convolution to enhance the weak emission at outer parts of the nebula; the effective seeing (after the smoothing) is $1.''1$ FWHM. The total magnitude of the nebula is $V = 22.6 \pm 0.3$. It is clearly shown that our V -band image reveals widely extended nebula component, showing remarkable contrast with the continuum emission, which is tightly aligned to the narrow radio jet (vO96; Pentericci et al. 1999). Note also that the V -band image appears very similar to the $\text{Ly}\alpha$ image taken with a narrow-band filter (vO96) and thus our V -band imaging traces the $\text{Ly}\alpha$ mostly. However, there is a notable difference between the two at northwest (NW) of the nucleus: Although the $\text{Ly}\alpha$ image shows an extended $\text{Ly}\alpha$ emission only toward southeast (SE) of the nucleus, our V -band image shows an extended nebula toward both NW and SE of the nucleus. Since our V -band filter bandpass covers the whole redshifted $\text{Ly}\alpha$ emission, and the contribution of the continuum emission should be almost negligible for the extended component judging from both the prominent nuclear source and weak emission extended along the jet (vO96; van Breugel et al. 1998; Pentericci et al. 1999), our V -band image and the $\text{Ly}\alpha$ image of vO96 should reveal the gaseous nebula in a similar way. Therefore this apparent discrepancy in two images needs an explanation.

Our $\text{Ly}\alpha$ spectrogram is shown in Figure 2 along with the slit position overlaid on our V -band image. The spectrogram is also smoothed by 4 by 4 binned-pixel running averaging

to enhance the outer weak emission. After the smoothing, the effective resolution is $1.''2$ in space, which is almost comparable to that of the smoothed imaging data. The velocity resolution is 600 km s^{-1} . In order to check the consistency quantitatively between the spectrogram and the V -band image, we made an one-dimensional plot of the spatial $\text{Ly}\alpha$ flux distribution by integrating the V -band flux over an expected slit position along the slit width directions (Figure 2b). A similar plot was also made from the spectroscopic data by integrating the flux on the spectrogram along the wavelength direction at each spatial position (Figure 2d). These two plots look very similar to each other; i.e., both show not only an asymmetric distribution toward SE but also a diffuse extension toward NW at a fainter flux level. This suggests not only that our spectroscopy and imaging data are consistent with each other (i.e., the spatial orientation of the spectrogram is right, and the slit was placed at the expected position at the center of the nebula), but also that the NW nebula does exist. It seems noteworthy that the NW component is blueshifted at 5541\AA or bluer for the most part (Figure 2c). Such a blueshifted component could not be detected by vO96 due to rather narrow wavelength coverage of their narrow-band filter ($5541\text{\AA} - 5601\text{\AA}$). Therefore, we conclude that there is a pair of elongated nebulae along NW and SE directions around 1243+036.

3.2. Description of $\text{Ly}\alpha$ Spectrogram

Our $\text{Ly}\alpha$ spectrogram (Figure 2c) reveals complicated structures of the nebula both in space and in velocity. We group the nebula into the following four components: (I) the compact nucleus component, (II) the extended near-systemic component at both sides of the nucleus, (III) the redshifted component aside the nucleus, and (IV) the extended blue components at both sides of the nucleus. We give below a summary of their observational properties and their comparisons with results of vO96, who conducted similar long-slit spectroscopy. Note that, although the slit position (centered on the nebula) and its orientation ($\text{PA}=152^\circ$) are the same for the two, the slit widths ($2.''5$ for vO96 and $0.''8$ for us) and the velocity resolutions (150 km s^{-1} for vO96 and 600 km s^{-1} for us) are different.

(I) The component at $< \pm 1''$ around the peak of the $\text{Ly}\alpha$ emission shows an evident blue-asymmetric profile with its peak at 5560\AA , being consistent with the report by vO96 (at 5557\AA). Its intensity peak corresponds spatially to that of the rest UV-optical continuum emission with which the radio core showing flatter spectrum is associated (vO96; van Breugel et al. 1998; Pentericci et al. 1999). Therefore, we attribute this component to the nucleus component. The blue wing emission can be traced down to -1400 km s^{-1} in the rest frame of the galaxy (hereafter all velocities are shown with respect to the systemic velocity in the

rest frame of the galaxy) although a part of the wing may be contaminated by the off-nucleus blue components at both sides of the nucleus (see below).

(II) The extended component whose velocity is close to the systemic one is found at both sides of the nucleus, and can be traced out to $\pm (4\text{--}5)''$ from the nucleus. It shows no strong velocity shear across the extension ($< 600 \text{ km s}^{-1}$) although the sky emission at 5577\AA might affect the measurement of its velocity curve given our lower velocity resolution. The velocity width is narrower than the nucleus component across the extension since we could not resolved the width by our instrument resolution (600 km s^{-1} FWHM).

vO96 detected an “outer halo” component extending out to $\pm 10''$ on both sides of the nucleus at almost systemic velocity. This component has a narrow line width ($\simeq 250 \text{ km s}^{-1}$ FWHM) and shows a large-scale velocity shear of as much as $\pm 225 \text{ km s}^{-1}$. Although our spectroscopic resolution is not high enough to investigate such a velocity curve, our near-systemic component appears to correspond to the outer halo component of vO96 although we detect it only out to $\pm 4 - 5''$.

(III) The redshifted component is detected at $\simeq 1''$ NW of the nucleus ³, and is found at redward of the sky emission. Due to the strong sky contamination, little information is available for this component.

(IV) The blueshifted component at SE extends up to $2''$ from the nucleus and shows strong blue-shifted velocity of $\simeq -1000 \text{ km s}^{-1}$. At the opposite side of the nucleus (NW), another blue component is detected which is much more extended ($\simeq 4'' - 5''$ from the nucleus) and shows much wider velocity width ($\simeq 1900 \text{ km s}^{-1}$ FWHM corrected for the instrumental resolution⁴). The velocity curve shows the bluest velocity of -1400 km s^{-1} at $\simeq 2.''5$ NW, and the velocity slows down at outer regions ($\simeq -1000 \text{ km s}^{-1}$ at $\simeq 5''$ NW).

vO96 has also detected blueshifted and extended component. Note, however, that there might be a difference between their spectrogram and ours. We could not detect any compact emission-line component at $\sim 2''$ NW from the nucleus ⁵, although vO96 claimed a presence

³Note that similar redshifted component is detected at $\simeq 1''$ SE of the nucleus (i.e., another side of the nucleus) in Figure 11 of vO96.

⁴Hereafter all line widths are given by a FWHM corrected for the instrumental resolution.

⁵We found that the spectrogram presented in vO96 (their Figure 11) is probably shown in wrong spatial direction (i.e., the spatial axis is flipped around the nucleus). This idea is based on the facts that (1) the redshifted component (III) is found at NW of the nucleus in our spectrogram, rather than at SE of the nucleus at a similar velocity, and (2) our *V*-band image and spectrogram are consistent with each other in orientation, as shown in section 3.1, and our *V*-band image and their narrow-band Ly α image (their Figure 9) are also consistent with each other in orientation, given the different wavelength coverage of the nebula

of an enhanced $\text{Ly}\alpha$ emission there which shows blueshifted velocity of -1100 km s^{-1} with a wider line width of 1200 km s^{-1} FWHM. Our spectrogram shows, on the other hand, a component which shows similar kinematical properties (blueshifted by $-1000 - -1400 \text{ km s}^{-1}$ with an even wider line width of 1900 km s^{-1} FWHM) but is extended more smoothly over $\simeq 4''$. This difference could be explained by the different slit coverage on the nebula between the two spectrograms, i.e., our narrow slit ($\simeq 1/3$ of vO96's) could not cover a portion of the nebula where enhanced $\text{Ly}\alpha$ emission is present. If this is the case, the nebula might have complex sub-structures within a nebula.

4. DISCUSSION

4.1. Origin of the $\text{Ly}\alpha$ nebula

We discuss plausible origins of the alignment effect observed in 1243+036. There are some pieces of evidence indicating that other mechanism than the radio-jet related one works to excite the extended nebula in 1243+036. First, the previous high-resolution images of R -band, K_s -band, and narrow-band near $2.3\mu\text{m}$ (corresponding to the rest-frame UV-optical continua and redshifted $[\text{OIII}]\lambda 4959, 5007\text{\AA}$ emission line, respectively) have revealed closely-aligned continuum and line emission along the narrow channel of the radio jet (van Breugel et al. 1998; Pentericci et al. 1999). Although this indicates an importance of the radio jet activity to the alignment effect, the $\text{Ly}\alpha$ nebula of this galaxy is extended much more widely than the region of the aligned continuum (Figure 1). Second, the extended components are blueshifted at both side of the nucleus. The jet-induced extranuclear shock, if any, should show a pair of blueshifted and redshifted components at each side of the nucleus because the symmetric propagation of a pair of jet and its counter jet is expected, being inconsistent with the observation. Therefore it seems very likely that the effect of the radio jet onto the extended nebula can not explain the excitation of the whole $\text{Ly}\alpha$ nebula.

Another idea of the origin of the widely extended $\text{Ly}\alpha$ nebula is the circumgalactic matter ionized by the anisotropic hard radiation from AGN. If this is the case, the matter irradiated by the AGN radiation is required to be distributed over a large scale ($\simeq 60 \text{ kpc}$) at a violent kinematical status to explain the velocity shift of $\simeq -1000 \text{ km s}^{-1}$ together with a large velocity dispersion of $1000 - 2000 \text{ km s}^{-1}$. One possibility may be that such violent gaseous systems are tidally-induced structures formed through a putative merger

(as explained in section 3.1), ensuring that our orientation is right. Therefore, although vO96 claimed that this high-velocity component is found at SE, its correct position is probably at the opposite side (NW) of the nucleus. In the following, we assume an image flip of the vO96's spectrogram for the comparison.

event. However, even nearby luminous mergers show an overall velocity differences of $\simeq 600$ km s $^{-1}$ or less along the tidal tails (e.g., Hibbard & Yun 1999; Mihos & Bothun 1998). Also the wider velocity dispersion seems difficult to be reproduced along the tidal tail (e.g., Hibbard & Yun 1999; Mihos & Bothun 1998). Another candidate for the extended matter is the remaining sub-galactic clumps for the galaxy formation. However, the range of the clump velocity dispersion would be 300 km s $^{-1}$ or less because gaseous clumps with a higher velocity dispersion are difficult for them to assemble to form a galaxy. Therefore this idea could not be simply applied for the case of 1243+036.

An alternative idea for the origin of the blue-shifted extended Ly α nebula is the shock-excited nebula associating with the superwind outflow. Our V-band image reveals a pair of elongated bubbles or cone-like structures extending into opposite ways from the nucleus. Similar extended nebulae are often seen around the starburst galaxies with the superwind/superbubble activity, such as M82, NGC 3079, and Arp 220 (e.g., Heckman et al. 1990). Also similar nebula is found around a high- z ($z = 2.4$) radio galaxy MRC 0406-244 which shows a pair of shock-excited elongated bubbles associated with the superwind activity (Taniguchi et al. 2001 and references therein). If 1243+036 is also the case, the projected velocity field of the nebula would show two components at different velocities each of which corresponds to either front or rear surface of the expanding bubble or outflowing cone (e.g., Heckman et al. 1990), rather than a single blueshifted component as observed. If the galaxy is surrounded by the dusty halo, which is often found around HzPRGs (van Ojik et al. 1997), the redshifted emission from the rear surface of the bubble may be attenuated due to the longer path through the halo. It seems also possible that the strong sky contamination at just red side of the Ly α emission might make it very difficult to detect redshifted counterparts of the blueshifted extended components. Therefore the blueshifted and extended components at both sides of the nucleus can be explained by the expanding bubble/outflowing cone model. The top of the expanding bubble, if not blown out to form conical outflow (e.g., Heckman et al. 1990), will show a single line-of-sight velocity. If the superbubble around 1243+036 expands almost within the sky plane, then the observed velocity would be blueshifted from the systemic velocity within the bubble, and it goes back closer to the systemic one at the tip. Wider velocity width may be due to the kinematical disturbance at the shock front of the bubble. Since the superwind/superbubble model can reproduce the observed morphological and kinematical properties of the nebula in qualitative ways, this model seems more plausible than the model of irradiated disturbed matter by AGN. Although we could not reject a possibility of the contribution of the AGN excitation to the nebula, it seems very likely that the superwind activity still plays an important role to bring the disturbed material around the galaxy as observed.

4.2. The superwind model

We apply a simple superwind model to the nebula around 1243+036 to see whether the observed size and the kinematical conditions can be reproduced quantitatively by the model. To estimate order-of-magnitude values of the nebula size and the expansion velocity, we apply a simple model of the evolution of a single spherical superbubble. The radius and the velocity of the expanding shell at time t_8 (in units of 10^8 yr) in the model are

$$r_{\text{shell}} \sim 110 L_{\text{mech},43}^{1/5} n_{\text{H},-5}^{-1/5} t_8^{3/5} \text{ kpc} \quad (1)$$

and

$$v_{\text{shell}} \sim 650 L_{\text{mech},43}^{1/5} n_{\text{H},-5}^{-1/5} t_8^{-2/5} \text{ km s}^{-1} \quad (2)$$

where $L_{\text{mech},43}$ is the mechanical luminosity released collectively from the supernovae in the central starburst in units of $10^{43} \text{ erg s}^{-1}$, and $n_{\text{H},-5}$ is the average hydrogen number density of the inter galactic medium (IGM) in units of 10^{-5} cm^{-3} (McCray & Snow 1979; Koo & McKee 1992a, 1992b; Heckman et al. 1996). Since the host galaxy is luminous in blue in the rest-frame of the galaxy ($M_B = -25.4$; van Breugel et al. 1998), it seems to be a massive elliptical galaxy with a mass $\sim 10^{12} M_\odot$. Assuming an instantaneous burst of star formation of $10^{11} M_\odot$, the mechanical luminosity is estimated to $L_{\text{mech}} \sim 10^{44} \text{ erg s}^{-1}$ over a time scale of $\gtrsim 10^7$ yrs (Leitherer et al. 1999)⁶. The average hydrogen number density of the IGM is estimated following Taniguchi & Shioya (2000), and is $1.1 \times 10^{-4} h^{-2} = 4.4 \times 10^{-4}$ at $z = 3.6$ in the adopted cosmology. Substituting all these values into the equations, we find $r_{\text{shell}} \simeq 80 t_8^{3/5} \text{ kpc}$ and $v_{\text{shell}} \simeq 480 t_8^{-2/5} \text{ km s}^{-1}$. Therefore both the observed size of the blueshifted extended nebula ($\simeq 30 \text{ kpc}$ in radius, corresponding to $4.5''$) and the maximum blueshift velocity (-1400 km s^{-1}) can be roughly reproduced if we assume $t_8 \simeq 0.1 - 0.3$, which is comparable to the age of a nearby superwind nebula of Arp 220 (e.g., Heckman et al. 1996). Hence the superwind model can be applicable to the blueshifted extended nebula of 1243+036 in a quantitative way.

5. Summary and Concluding Remarks

We found an elongated giant nebula ($\sim 60 \text{ kpc}$) with blueshifted ($-1100 - -1400 \text{ km s}^{-1}$) and broad ($\simeq 1000 - 1900 \text{ km s}^{-1}$ FWHM) Ly α emission around a HzPRG 1243+036 at

⁶Although the estimate of the mechanical luminosity depends strongly on the choice of the shape of the stellar initial mass function (upper- and lower-mass cut-offs and slope of the function) and metallicity as well as the mass of the burst, and is difficult to be made accurately, results of the model calculation are not sensitive to the adopted mechanical luminosity since both r_{shell} and v_{shell} are proportional to just one fifth power of $L_{\text{mech},43}$.

$z = 3.6$. The nebula can be recognized as a pair of expanding elongated bubbles or outflowing bi-directional cones at both sides of the nucleus, being much similar to some prototypical superwind galaxies in local universe in both morphological and kinematical points of view. We show that the superwind model can be applicable to the nebula to explain the size and the kinematical properties of its bubble or cone-like structure.

In order to see such an evolved nebula associated with the superwind activity at $z = 3.6$, the onset of the starburst should be at $z = 5 \sim 7$. This is because it takes several 10^8 yrs for the superwind to blow out of the host galaxy since the onset of the burst (Arimoto & Yoshii 1987), and another a few 10^7 yrs is required for the nebula to expand to the observed size. If this would be the case, it seems very likely that 1243+036 is in the phase of the galactic wind after the initial burst for the galaxy formation (Arimoto & Yoshii 1987).

We thank L. Pentericci for her valuable comments and suggestions to improve this paper.

REFERENCES

- Arimoto, N., & Yoshii, Y. 1987, *A&A*, 173, 23
- Chambers, K. C., Miley, G. K., & van Breugel, W. 1987, *Nature*, 329, 604
- Chambers, K. C., Miley, G. K., & van Breugel, W. J. M. 1990, *ApJ*, 363, 21
- Chevalier, R. A., & Clegg, A. W. 1985, *Nature*, 317, 44
- Cimatti, A., di Serego Alighieri, S., Vernet, J., Cohen, M., & Fosbury, R. A. E. 1998, *ApJ*, 355, 416
- De Breuck, C., Röttgering, H., Miley, G., van Breugel, W., & Best, P. 2000, *A&A*, 362, 519
- De Breuck, C., van Breugel, W., Stanford, S. A., Röttgering, H., Miley, G., & Stern, D. 2002, *AJ*, 123, 677
- Dickson, R., Tadhunter, C., Shaw, M., Clark, N., & Morganti, R. 1995, *MNRAS*, 273, L29
- di Serego Alighieri, S., Fosbury, R. A. E., Tadhunter, C. N., & Quinn, P. J. 1989, *Nature*, 341, 307
- Dey, A., van Breugel, W., Vacca, W. D., & Antonucci, R. 1997, *ApJ*, 490, 698
- Fabian, A. C. 1989, *MNRAS*, 238, 41p
- Heckman, T. M., Armus, L., & Miley, G. K. 1990, *ApJS*, 74, 833
- Heckman, T. M., Dahlem, M., Eales, S. A., Fabbiano, G., & Weaver, K. 1996, *ApJ*, 457, 616

- Hibbard, J. H., & Yun, M. S. 1999, *AJ*, 118, 162
- Kaifu, N. 1998, *Proc. SPIE*, 3352, 14
- Kashikawa, N., et al. 2002, *PASJ*, 54, 819
- Koo, B. -C., & McKee, C. F. 1992a, *ApJ*, 383, 93
- Koo, B. -C., & McKee, C. F. 1992b, *ApJ*, 388, 103
- Lacy, M., Miley, G., Rawlings, G., et al. 1994, *MNRAS*, 271, 504
- Leitherer, C., Schaerer, D., Goldader, J. D., Delgado, R. M. G., Robert, C., Kune, D. F., de Mello, D. F., Devost, D., & Heckman, T. M. 1999, *ApJS*, 123, 3
- McCarthy, P. J., van Breugel, W. J. M., Spinrad, H., & Djorgovski, S. G. 1987, *ApJ*, 321, L29
- McCarthy, P. J. 1993, *ARA&A*, 31, 639
- McCray, R., & Snow, T. P. 1979, *ARA&A*, 17, 213
- Mihos, J. C., & Bothun, G. D. 1998, *ApJ*, 500, 619
- Pentericci, L., Röttgering, H. J. A., Miley, G. K., McCarthy, P., Spinrad, H., van Breugel, W. J. M., & Macchetto, F. 1999, *A&A*, 341, 219
- Pentericci, L., McCarthy, P. J., Röttgering, H. J. A., Miley, G. K., van Breugel, W. J. M., & Fosbury, R. 2001, *ApJS*, 135, 63
- Röttgering, H. J. A., Lacy, M., Chambers, K. C., & Saunders, R. 1994, *A&AS*, 108, 79
- Röttgering, H. J. A., Miley, G. K., Chambers, K. C., & Nacchetto, F. 1995, *A&AS*, 114, 51
- Röttgering, H. J. A., van Ojik, R., Miley, G. K., Chambers, K. C., van Breugel, W. J. M., & de Koff, S. 1997, *A&A*, 326, 505
- Rush, B., McCarthy, P. J., Athreya, R. M., & Persson, S. E. 1997, *ApJ*, 484, 167
- Strickland, D. K., & Sutherland, I. R. 2000, *MNRAS*, 314, 511
- Taniguchi, Y., Ohyama, Y., Murayama, T., et al. 2001, *ApJ*, 559, L9
- Taniguchi, Y., & Shioya, Y. 2000, *ApJ*, 532, L13
- Yoshida, M., et al. 2000, *SPIE*, 4009, 240
- van Breugel, W. J. M., Stanford, S. A., Spinrad, H., Stern, D., & Grapham, J. R. 1998, *ApJ*, 502, 614
- van Breugel, W., De Breuck, C., Stanford, S. A., Stern, D., Röttgering, H., & Miley, G. 1999, *ApJ*, 518, L61

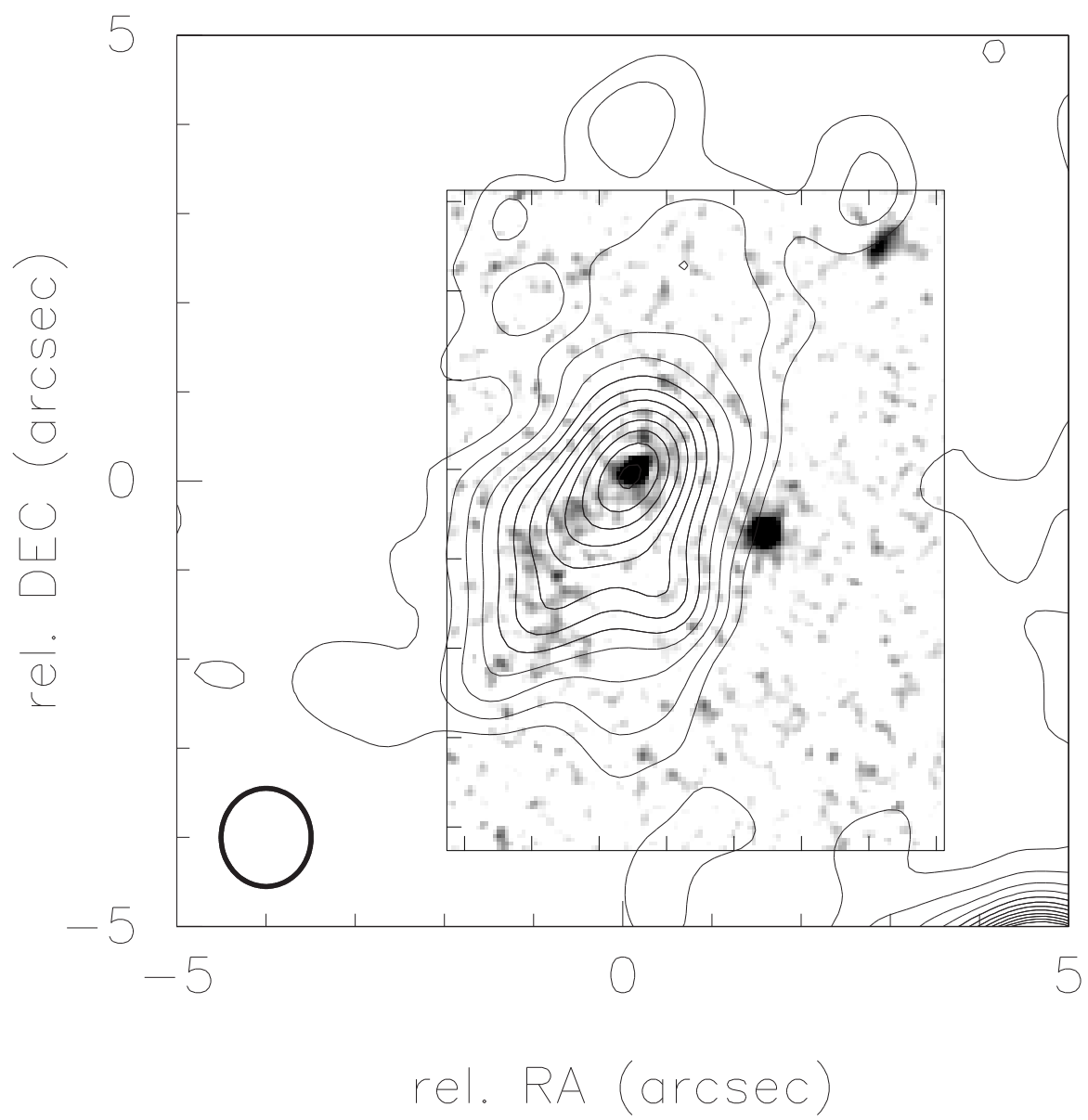
van Ojik, R., Röttgering, H. J. A., Carilli, C. L., Miley, G. K., Bremer, M. N., & Macchetto, F. 1996, *A&A*, 313, 25 (vO96)

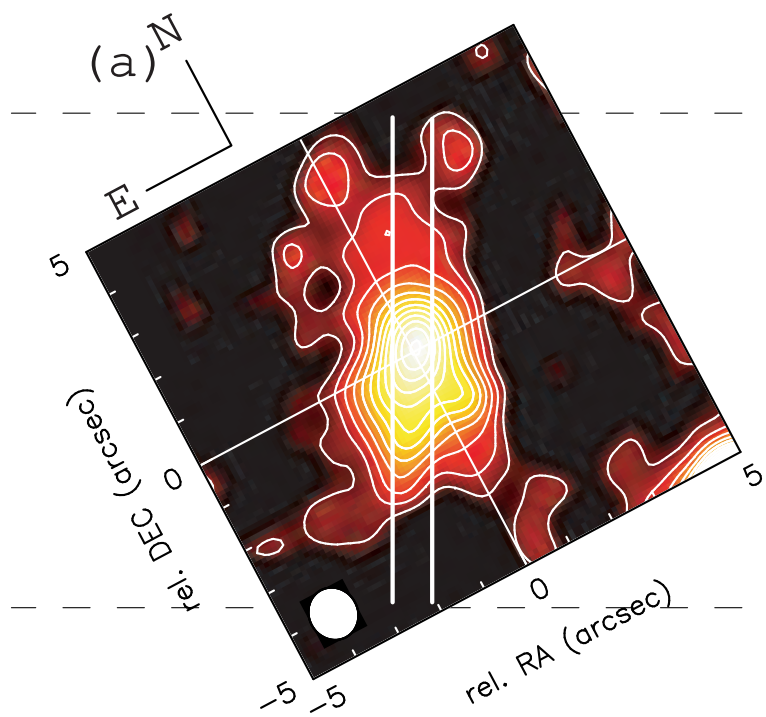
van Ojik, R., Röttgering, H. J. A., Miley, G. K., & Hunstead, R. W. 1997, *A&A*, 317, 358

Villar-Martín, M., Alonso-Herrero, A., di Serego Alighieri, S., & Vernet, J. 2000, *A&AS*, 147, 291

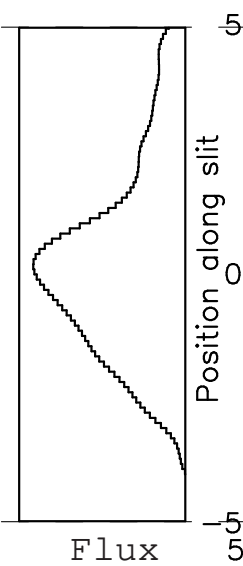
Fig. 1.— Our *V*-band image (contours) and a HST F702W image of Pentericci et al. (1999) (gray scale) are compared. North is up and east is to the left. Relative coordinates from the nucleus are shown in both RA and Dec. The lower-left circle represents our effective seeing size after Gaussian smoothing ($1.1''$ FWHM). The object at $\sim 2''$ southwest of the nucleus may not be part of the system (van Breugel et al. 1998). Lower right contours seen in *B*-band image is of a nearby bright star.

Fig. 2.— A *V*-band image and $\text{Ly}\alpha$ spectrogram of 1243+036. (a) *V*-band image after smoothing by the Gaussian convolution. The effective seeing size after the smoothing size is $1.1''$ FWHM, and is shown by the lower-left circle. Lower right emission is a part of the nearby bright star. The image is rotated so that the slit ($0.8''$ width, at $\text{PA}=152^\circ$) is shown vertically on it (with two vertical lines at the center). (b) One-dimensional *V*-band flux distribution along the slit. (c) $\text{Ly}\alpha$ spectrogram after averaging over 4×4 binned-pixel averaging. Vertical axis is for spatial direction (upper side is toward northwest and lower side is toward southeast), and horizontal axis is for wavelength direction (right side is toward red). The region contaminated by the strong sky emission at 5577\AA is not shown, and is marked in blue. (d) One-dimensional $\text{Ly}\alpha$ flux distribution along the slit.

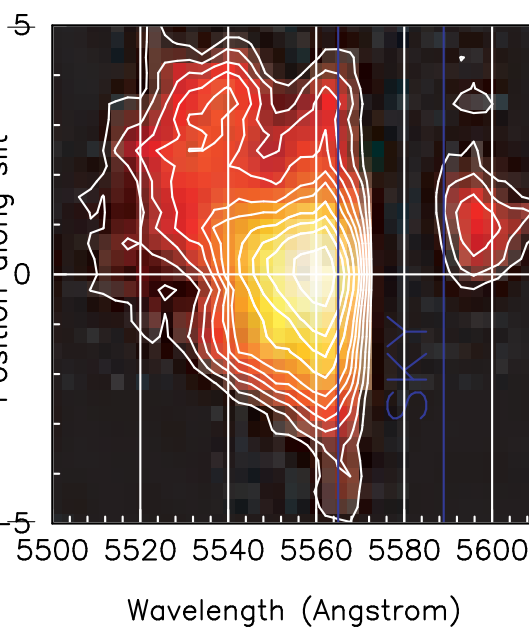




(b)



(c)



(d)

